UNIGNITED HIGH-PRESSURE METHANE JET IMPACTING A CYLINDRICAL OBSTACLE: AN ASSESSMENT TOOL FOR RISK ANALYSIS

Cristian Colombini[a,b], Clara Iannantuoni[a], Renato Rota[a], Valentina Busini[a,*]

[a] *Politecnico di Milano - Department of Chemistry, Materials and Chemical Engineering "Giulio Natta", Piazza Leonardo da Vinci 32, 20133, Milano, Italy*
[b] *EOGHR (Oil & Gas HSE & Reliability) - RINA Consulting S.p.A., Via Cecchi 6, 16129 Genova, Italy*

* Corresponding author:

E-mail address: valentina.busini@polimi.it

ABSTRACT

In the Oil & Gas sector, the use of flammable substances stored and transported in gaseous form and under pressure conditions is quite common. In the field of industrial safety, high-pressure gaseous releases of a flammable material impacting an obstacle are of paramount importance, as possible accidental scenarios, due to their catastrophic consequences. Although hot release (*i.e.,* jet fire scenarios) is a topic that has been largely covered in literature, cold releases (*i.e.,* unignited flammable releases) did not. This gap increases when considering high-pressure cold releases interacting with an obstacle. Being a probable situation when an accidental high-pressure loss of containment occurs, the need of reliable as well as quick tools for prompt safety evaluations of the hazardous area of this kind of scenario is of primary importance. To this aim, the present work proposes such an assessment tool derived from an extensive CFD analysis of several possible situations of a cylindrical obstacle impinged by an unignited high-pressure gaseous methane jet.

KEYWORDS

High-pressure release; methane; cylindrical obstacle; risk assessment; CFD; practical tool

ACRONYMS

CFD Computational fluid Dynamics

EDM Equivalent Diameter Model

FF Flash Fire

HP High-Pressure

JF Jet Fire

LFL Lower Flammability Limit

LPG Liquefied Petroleum Gas

ME Maximum Extent

O&G Oil and Gas

RANS Reynolds Averaged Navier-Stokes

TKE Turbulent Kinetic Energy

NOMENCLATURE

A_{PS}: pseudo-source area extension

c: methane concentration in air

c_{ax}: methane concentration along the free jet axis

C_D: discharge coefficient

d: actual orifice diameter

D: distance of the center of the cylindrical obstacle from the jet source

d_{FJ}: free jet diameter

d_{PS}: pseudo-source orifice diameter

D_O: obstacle diameter

H_N: jet source height

H_O: height of the vertical cylindrical obstacle

k: axial decay constant

L_O: length of the horizontal cylindrical obstacle

ME: jet axial maximum extent

ME_{FJ}: free jet maximum extent in direction of the jet axis

MW: methane molar weight

$\dot{m}_{PS}$: pseudo-source mass flow rate

p: upstream methane pressure

p_{amb}: ambient pressure

R: universal gas constant

T: upstream methane temperature

T_{amb}: ambient static temperature

T_{PS}: methane static temperature at pseudo-source conditions

v_{PS}: methane velocity at pseudo-source conditions

γ: specific heat ratio

ρ_{PS}: methane density at pseudo-source conditions

ρ_{amb}: air density

1. INTRODUCTION

In the Oil & Gas (O&G) sector, the use of flammable substances stored and transported in gaseous form and under pressure conditions is quite common (Varsegova et al., 2019; Khraisheh et al., 2020; Zhang et al., 2020; Zhu et al., 2020). In the field of industrial safety, high-pressure (HP) releases of a flammable material impacting an obstacle are of paramount importance as possible accidental scenarios (Rian et al., 2016; Jang et al., 2016; Hall et al., 2017; Kotchourko et al., 2014). Fundamentally, the reasons of such an importance are:

- the scenario occurrence probability: any process, chemical and O&G plant is full of potential obstacles located in the vicinity of a potential source of a high-pressure release (Casal et al., 2012; Xu et al., 2011; Jang et al., 2016; Colombini and Busini, 2019b)
- the increased damage area (Hall et al., 2017; Pontiggia et al., 2014; Kotchourko et al. 2014)
- the ignition possibility of the release (Houf and Schefer, 2007; Darbra et al., 2010; Woodward and Pitblado, 2010)

Therefore, the resulting Flash Fire (FF) may involve a larger area with respect to the case of open field conditions (*i.e.*, the free jet scenario). A greater chance of involving neighbouring structures, triggering the well-known domino effect (which leads to the catastrophic consequences as documented in literature (Casal, 2008; Benard et al., 2009; Darbra et al., 2010)), would be, thus, a concrete risk to be considered. Focusing on different realistic accidental scenarios, several researches have pursuit the aim of estimating the hazardous distance related to HP releases both experimentally and numerically. Benard et al. (2007) compared how two Computational Fluid Dynamics (CFD) software and one simpler tool predict the size of the flammable cloud of hydrogen and methane high-pressure releases when bounded by a surface. Tchouvelev et al. (2007) applied the CFD to study how a small protective wall can reduce the clearance distances of an impingent unignited high-pressure hydrogen jet. Desilets et al. (2009) performed an experimental campaign, and a further CFD analysis, of low-pressure hydrogen jets with the aim to define the effect that a nearby flat surface has on both shape and size of the cloud. Benard et al. (2009) analyzed the effect that a horizontal flat surface has on both methane and hydrogen jets. Considering two different storage pressure and several distances of the source from the surface. Hourri et al. (2009) investigated numerically the effect that the ground and a side wall have on methane and hydrogen unignited high-pressure jets. The aim has been to compare how gases with different behaviour, released from sources with different orientations, are affected by the solid surface. Houf et al. (2010) evaluated the mitigation capability of different configurations of barrier walls on

unintended ignited and unignited hydrogen high-pressure jets. Hourri et al. (2011) studied the increasing effect that a horizontal surface has on the damage area of horizontal methane and hydrogen unignited high-pressure jets. They compared the results of two CFD software, in predicting both the size and the shape of the Lower Flammability (LFL) cloud. In the same year, Angers et al. expanded the analysis of Hourri et al. (2011) to the case of vertical flat surfaces influencing methane and hydrogen high-pressure jets. Pontiggia et al. (2014) compared the results obtained with a CFD code and an integral model in predicting the maximum extent of the LFL cloud for a realistic case study in which a high-pressure methane jet impinges an obstacle. In 2016, from an extensive CFD analysis performed with FLACS, Benard et al. derived engineering correlations for predicting the maximum extent of the lower flammability limit cloud; the work considered both hydrogen and methane high-pressure jets when influenced by a parallel surface. Similarly to Pontiggia et al. (2014), Gerbec et al. (2017) compared the results of an integral model to the ones of CFD simulations in order to show their capability of modeling the realistic scenario of a Liquefied Petroleum Gas (LPG) release due to the overfill of a car tanker. They showed that the integral model overestimates the damage area. Hall et al. (2017) performed an extensive experimental campaign focused on collecting data about the effect that the ground and a ceiling have on HP hydrogen jets. Colombini and Busini (2019a and 2019b) have studied numerically how a realistic obstacle (namely, a cylindrical tank oriented horizontally and vertically) can modify the lower flammability limit cloud of an unignited HP methane jet as function of some of the geometrical parameters of the scenario.

From the literature works, we can notice that only three studies have been performed experimentally and most of the numerical works are CFD-based since CFD is the only numerical tool able to account for any kind of geometrical complexities (Batt et al., 2016).

Despite its large use, in industrial risk assessment activities, especially during the design and construction phases, CFD simulations still present their limits of application, mainly because their computational costs (Uggenti et al., 2017).

In this context, as remarked by Derudi et al. (2013) and Kotchourko et al. (2014), a simple tool that, for instance, allows to distinguish the cases which require CFD and which do not, would be useful for the specialists that are involved in consequence analysis activities. To the best of authors' knowledge, such information is not available for scenarios involving flammable HP jets impacting a cylindrical obstacle.

Therefore, in this work, a realistic accidental high-pressure jet-obstacle scenario was analysed: an unignited HP methane release impinging a cylindrical obstacle. The CFD was used to simulate a large number of configurations by changing: the distance between the methane HP source and the obstacle; the methane storage pressure; the obstacle diameter; the observed methane concentration in air and the obstacle orientation. As main achievement of the work, we propose a simple analytical tool that permits to assess how the accidental HP jet is influenced by the obstacle presence.

2. MATERIALS AND METHODS

To carry out the simulations, the CFD tool was coupled with the so-called Equivalent Diameter Model (EDM) for modeling the high momentum source term. Through this approach, less computational efforts are needed keeping anyway the results reliability (Hess et al., 1973; Sposato et al., 2003; Pontiggia et al., 2014; Benard et al., 2007; Houf et al., 2007; Deng et al., 2018; Stewart et al., 2019; Tolias et al., 2019). It consists of modeling the jet source with a thermodynamics-based model, therefore avoiding the simulation of the physical phenomena relative to the supersonic release. In the present work, the model developed by Birch et al. (1984) was chosen. Table 1 in the following reports the main characteristics defining the pseudo-source as per Birch et al. (1984) EDM.

Table 1: Equations of Birch et al. (1984) EDM defining the pseudo-source of the jet. In the Equations, d_{PS} is the resulting diameter of the pseudo-source, d is the actual orifice diameter, C_D is the discharge coefficient, p is the storage pressure, p_{amb} is the environmental pressure, γ is the specific heat ratio, MW is the methane molar weight, $\dot{m}_{PS}$, v_{PS}, ρ_{PS}, T_{PS}, p_{PS} and A_{PS} are the resulting mass flow rate, velocity, density, static temperature, pressure and area extension of the pseudo-source, respectively. As indicated, methane density at the pseudo-source is computed based on the ideal gas Equation of state. Further details are provided in the work of Birch et al. (1984).

Pseudo-source characteristic	Equation
Equivalent diameter	$d_{PS} = d\sqrt{C_D\left(\frac{p}{p_{amb}}\right)\left(\frac{2}{\gamma+1}\right)^{\frac{(\gamma+1)}{2(\gamma-1)}}}$
Mass flow rate	$\dot{m}_{PS} = \rho_{PS} \cdot A_{PS} \cdot v_{PS}$
Density	$\rho_{PS} = \frac{p_{PS} \cdot MW}{R \cdot T_{PS}}$
Pressure	$p_{PS} = p_{amb}$
Static temperature	$T_{PS} = T_{amb}$

The software used to perform the CFD analysis was Ansys® Workbench® (release 19.1). The computational domain was sized following the work of Hourri et al. (2009), using a vertical planar symmetry along the jet axis. Then, the fluid volume discretization was realized. Focusing on the flow region in which large gradients values of the physical variables are expected, we exploited the body of influence feature to obtain a way less computationally expensive mesh. In particular, five different bodies placed along the jet axis were considered. With this approach, on one hand we avoided a useless dense mesh in correspondence of the domain outskirts; on the other hand, we obtained a high-degree refinement within the volume surrounding the jet axis. More details regarding this mesh strategy are reported elsewhere (Colombini et al., 2020a, Colombini et al., 2021c). A fully unstructured tetrahedral grid was obtained for all the considered configurations. Figure 1 shows an example of the mesh appearance. Quality requirements were always satisfied (*i.e.*, orthogonal quality and skewness). Moreover, the grid independence of the results was verified by considering two other mesh sizes for a reference configuration (namely, one larger and one smaller, obtained by halving and doubling the cell size along the jet axis, respectively). Figure 1S in the supplementary material shows the sensitivity analysis results in terms of jet maximum axial extent (*ME*) over the mesh refinements. This assessment was done considering scenario 18_M of Table 3. All the simulations were performed in steady state conditions and the pressure-based solver was chosen thanks to the equivalent diameter model deployment (allowing the flow to be treated as incompressible). RANS approach was used together with the two-equation eddy-viscosity k-ω SST model (Menter, 1993) and the ideal gas equation of state. For what concerns the numerical settings, the COUPLED pressure-velocity coupling scheme was adopted and the second order upwind spatial-discretization was considered for all the convective terms. Table 1S in the supplemental information reports the model equations together with the definition of the main parameters. Table 2 reports the boundary conditions used. Notice that constant wind intensity of 5 m/s was assumed parallel to the jet axis and blowing from back side (*i.e.,* z axis direction).

Table 2: Name, type and specifics of the boundary conditions used.

Boundary name	Type	Specifics
Back side	Velocity inlet	air, v_z = 5 m/s, T = 300 K
Top side	Velocity inlet	air, v_z = 5 m/s, T = 300 K
Left side	Velocity inlet	air, v_z = 5 m/s, T = 300 K
Ground	Wall	0.01 m roughness height, adiabatic
Symmetry	Symmetry	-
Front side	Pressure outlet	air, $T_{BACKFLOW}$ = 300 K
Nozzle	Wall	0.001 m roughness height, adiabatic
Methane jet	Mass flow inlet	Computed case by case according to Birch et

		al. (1984) model equations
Cylindrical obstacle	Wall	0.001 m roughness height, adiabatic

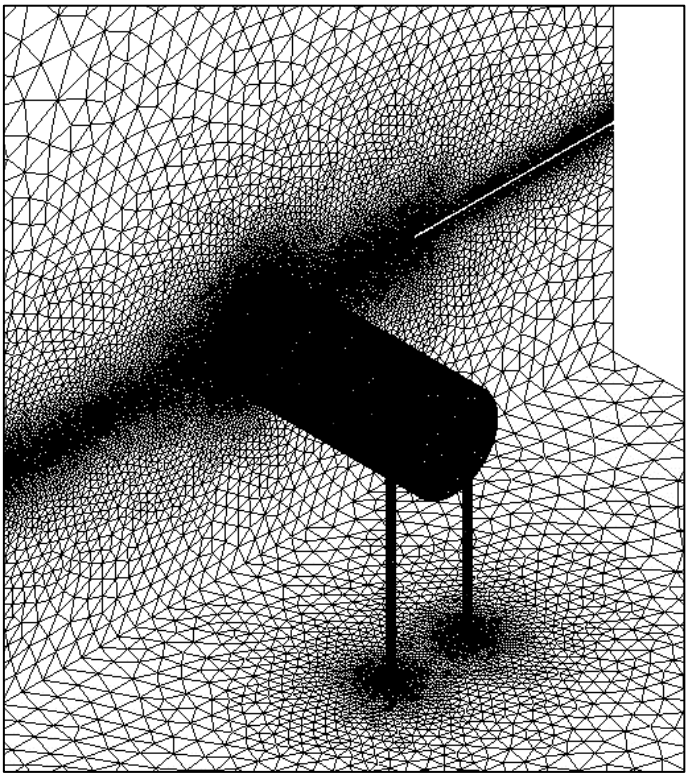

Figure 1: Example of obstacle, symmetry plane and ground surface grid for run 18_M.

3. RESULTS AND DISCUSSION

Further below, the extensive analysis of horizontal cylindrical obstacles effect on the jet development is described, the results obtained are discussed and a simple tool as the main outcome of the analysis is proposed. Then the analysis regarding the effect of the obstacle orientation (vertical vs. horizontal) is provided aiming to highlight how this aspect impacts the jet development.

3.1 HORIZONTAL CYLINDRICAL OBSTACLE ANALYSIS

Figure 2 shows a sketch of the scenario, where main geometric characteristics are defined. The methane high-pressure source was modelled using a nozzle, where the effective size of the jet source is computed exploiting the Birch et al. (1984) EDM. Assuming the obstacle to be located in an industrial area, the ground was considered as a concrete flat. The cylindrical obstacles were

considered with four legs. Because of the axial symmetry of the domain, only half of the obstacle was modelled. As mentioned, sizes of the computational domain were based on a literature work (Hourri et al., 2009); however, to avoid any unwanted effect related to the boundary conditions, some trials on the domain extents were preliminarily performed.

The influence of the cylindrical obstacle was investigated varying the distance between the methane HP source and the obstacle (*D*), the height of the source above ground (H_N), the methane storage pressure (*p*), the obstacle diameter (D_O), the observed methane concentration in air (*c*) and the obstacle orientation (horizontal or vertical). The variation of all these parameters has led to investigate several cases, defined accordingly to values reported in Table 3. In agreement with previous works (Colombini et al., 2019a; Colombini et al., 2019b; Colombini et al., 2020a; Colombini et al., 2020b; Colombini et al., 2021a), the axial maximum extent (*ME*) of the cloud was recorded to quantify the obstacle effect on the methane jet. Considering the horizontal obstacle case, the results obtained are reported in the last three columns of Table 3.

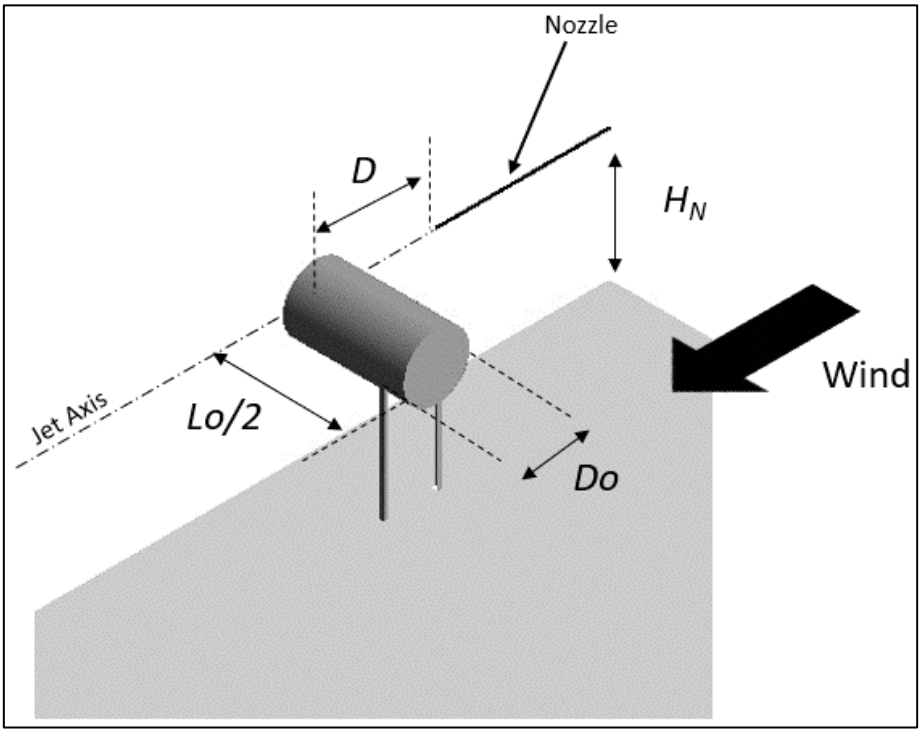

Figure 2: Sketch of the scenario. In the Figure, the vertical symmetry plane in correspondence of the jet axis defines the boundary of the domain.

Table 3: Values of the characteristics defining the cases simulated and results achieved for the horizontal obstacle case. Subscript x indicates the concentration level observed: x = L means c = 3.5%, x = M means c = 5.3% (LFL) and x = H means c = 10%.

Run	*p*	*d*	d_{PS}	H_N	D_O	L_O	*D*	*ME* [m]

	[bar]	[m]	[m]	[m]	[m]	[m]	[m]	*x = L*	*x = M*	*x = H*
1_X	65	0.0254	0.146	6	2	11	2.93	13.7	9.4	5.45
2_X	65	0.0254	0.146	6	2	11	4.87	15.7	11.25	6.9
3_X	65	0.0254	0.146	6	2	11	6.81	18.25	13.3	8.15
4_X	65	0.0254	0.146	6	2	11	8.75	20.8	15.05	8.95
5_X	65	0.0254	0.146	6	2	11	10.68	23.3	16.45	8.45
6_X	65	0.0254	0.146	6	2	11	12.62	25.1	17.15	8.45
7_X	65	0.0254	0.146	6	2	11	14.56	26.4	17.15	8.45
8_X	65	0.0254	0.146	6	2	11	16.5	27.05	17.6	8.45
9_X	65	0.0254	0.146	6	3	11	3.43	12.6	8.7	5.05
10_X	65	0.0254	0.146	6	3	11	5.37	14.15	10.1	6.15
11_X	65	0.0254	0.146	6	3	11	7.312	16.7	12.15	7.5
12_X	65	0.0254	0.146	6	3	11	9.25	18.75	13.55	8.5
13_X	65	0.0254	0.146	6	3	11	11.18	19.9	14.25	8.45
14_X	65	0.0254	0.146	6	3	11	13.12	21.4	15.45	8.45
15_X	65	0.0254	0.146	6	3	11	15.06	22.8	16.2	8.45
16_X	65	0.0254	0.146	10	4.5	20	4.18	13.45	8.6	4.9
17_X	65	0.0254	0.146	10	4.5	20	6.12	14.25	9.8	5.9
18_X	65	0.0254	0.146	10	4.5	20	8.06	15.85	11.2	7.1
19_X	65	0.0254	0.146	10	4.5	20	10	16.65	12.65	8.3
20_X	65	0.0254	0.146	10	4.5	20	11.93	18.85	14.1	8.45
21_X	65	0.0254	0.146	10	4.5	20	13.87	20.4	15.1	8.45
22_X	65	0.0254	0.146	10	4.5	20	15.81	21.8	15.9	8.45
23_X	65	0.0254	0.146	10	4.5	20	17.75	22.9	16.5	8.45
24_X	65	0.0254	0.146	10	7.5	20	5.68	12.4	9.35	4
25_X	65	0.0254	0.146	10	7.5	20	7.62	13.15	9.45	5.1
26_X	65	0.0254	0.146	10	7.5	20	9.56	14.5	10.3	6.6
27_X	65	0.0254	0.146	10	7.5	20	11.5	16.2	11.4	8.1
28_X	65	0.0254	0.146	10	7.5	20	13.43	17.6	12.7	8.45
29_X	65	0.0254	0.146	10	7.5	20	15.37	18.9	13.9	8.45
30_X	65	0.0254	0.146	10	7.5	20	17.31	20	15.1	8.45
31_X	195	0.0254	0.252	10	3	20	3.43	21.8	13.6	7.6
32_X	195	0.0254	0.252	10	3	20	5.37	22.8	15.8	9.5
33_X	195	0.0254	0.252	10	3	20	7.31	25.2	18	11.1
34_X	195	0.0254	0.252	10	3	20	9.25	27.8	20.1	12.35
35_X	195	0.0254	0.252	10	3	20	11.18	30.7	22.3	13.45
36_X	195	0.0254	0.252	10	3	20	13.12	33.3	24.1	14.5
37_X	195	0.0254	0.252	10	3	20	15.06	36.1	25.8	14.8
38_X	260	0.0254	0.291	10	3	20	3.43	23.4	15.6	8.8
39_X	260	0.0254	0.291	10	3	20	5.37	26	17.9	10.65
40_X	260	0.0254	0.291	10	3	20	7.31	28.4	20	12.4
41_X	260	0.0254	0.291	10	3	20	9.25	31.4	22.4	13.9
42_X	260	0.0254	0.291	10	3	20	11.18	34.4	24.7	15.2
43_X	260	0.0254	0.291	10	3	20	13.12	37.4	26.9	16.2
44_X	260	0.0254	0.291	10	3	20	15.06	40.5	28.9	16.8
45_X	455	0.0254	0.385	10	3	20	3.43	32.35	20.5	10.4
46_X	455	0.0254	0.385	10	3	20	5.37	33.7	22.8	13.15

47_X	455	0.0254	0.385	10	3	20	7.31	36.5	25	15.2
48_X	455	0.0254	0.385	10	3	20	9.25	40.1	27.8	17.1
49_X	455	0.0254	0.385	10	3	20	11.18	43.7	30.5	19
50_X	455	0.0254	0.385	10	3	20	13.12	47.4	33.3	20.5
51_X	455	0.0254	0.385	10	3	20	15.06	51.4	36	21.8
52_X	650	0.0254	0.461	10	3	20	3.43	52.7	24	13.9
53_X	650	0.0254	0.461	10	3	20	5.37	38.7	25.9	14.9
54_X	650	0.0254	0.461	10	3	20	7.31	42.5	28.9	17.2
55_X	650	0.0254	0.461	10	3	20	9.25	47	32.1	19.5
56_X	650	0.0254	0.461	10	3	20	11.18	51	35.3	21.6
57_X	650	0.0254	0.461	10	3	20	13.12	55.5	38.8	23.6
58_X	650	0.0254	0.461	10	3	20	15.06	59.8	41.6	25.2

It is worthwhile noting that, the scope of the work was focused on studying obstacle related effect only. Thus, cases defined in Table 3 account only for obstacle influence and, in none of them, the ground effect is present.

To effectively compare the results and show how the cylindrical obstacle influences the impinging jet development in the situations defined in Table 3, the results computed were plotted in a suitable dimensionless space, that is, the ratio between the radial dimension of the free jet cloud evaluated in correspondence of the cylindrical obstacle centre position ($d_{FJ}(D)$) and the obstacle diameter (*Do*) vs. the ratio between *ME* and the same extension of the correspondent free jet (ME_{FJ}).

Figure 3 shows the results computed: independently by upstream pressure, obstacle diameter, distance of the obstacle from the source, and methane concentration the jet length is always lower than the maximum extent of the correspondent free jet and, only in few cases; the ME exceeds that of the free jet for no more than about 10%. In particular, the greater the concentration level, the shorter the jet extent is. Therefore, by order of magnitude, the results in the Figure show that the horizontal cylindrical tank limits the length of the jet cloud to values lower than or, at least, slightly larger than that of the correspondent free jet.

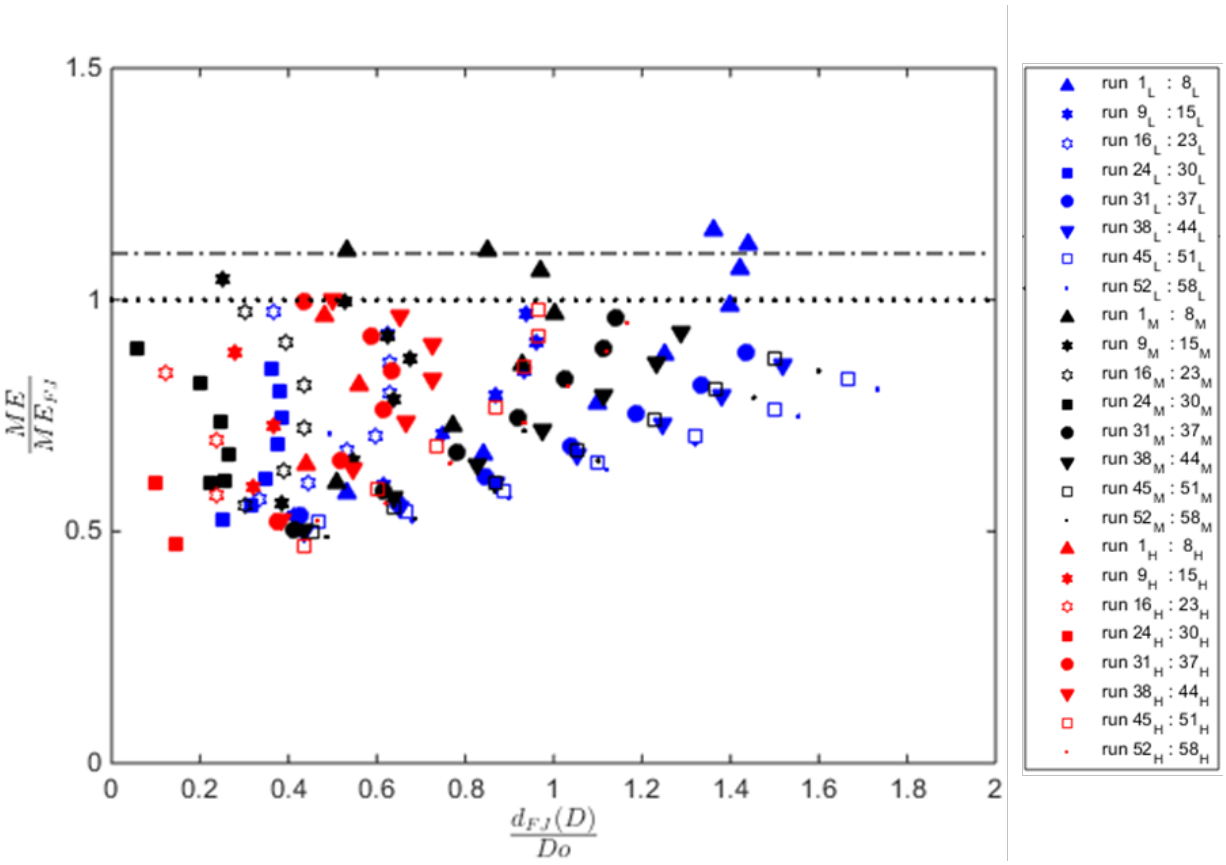

Figure 3: Results of runs in Table 3. Markers colour defines the methane concentration level observed: blue is for the low level (c = 3.5 %), black is for the mean level (c = 5.3 %) and red is for the high level (c = 10 %). The dotted line identifies when ME/ME_{FJ} = 1, while the dash dotted line when ME/ME_{FJ} = 1.1.

With regards to the Figure, it has to be noted that some results of Table 3 are missing. The reason lies in the fact that the obstacle position was too far from the HP source. For these cases, the radial extent of the free jet measured at a distance equal to the obstacle centre position (*D*) would be equal to zero, making it meaningless to be included in the plot. These are the 8 % of the total results computed. In Table 3, these runs are those for which the *ME* of jet is equal to the correspondent free jet extent (*i.e.,* 5_H, 6_H, 7_H, 8_H, 13_H, 14_H, 15_H, 20_H, 21_H, 22_H, 23_H, 28_H, 29_H, 30_H).

3.2 ANALYTICAL TOOL PROPOSAL

Based on the results exposed in previous Section, the main outcome of this work is the following by hand procedure that, by order of magnitude, provides an estimation of the *ME* of unignited methane high-pressure jets impinging horizontal cylindrical obstacles.

1. From the accidental release characteristics, estimate d_{PS} and ρ_{PS} value using the Birch et al. (1984) model:

$$d_{PS} = d\sqrt{C_D\left(\frac{p}{p_{amb}}\right)\left(\frac{2}{\gamma+1}\right)^{\frac{(\gamma+1)}{2(\gamma-1)}}}$$

$$\rho_{PS} = \frac{p_{PS} \cdot MW}{R \cdot T_{PS}}$$

$$p_{PS} = p_{amb}$$

$$T_{PS} = T_{amb}$$

where d_{PS} is the pseudo-source diameter, d is the actual orifice diameter, C_D is the source discharge coefficient, p is the upstream pressure, p_{amb} is the environmental pressure, γ is the specific heat ratio, ρ_{PS} is the methane density at pseudo-source conditions, p_{PS} is the methane pressure at pseudo-source conditions, MW is the methane molecular weight, R is the universal gas constant, T_{PS} is the methane static temperature at pseudo-source conditions, p_{amb} is ambient pressure, and T_{amb} is the ambient static temperature

2. Using the concentration decay model of Chen and Rodi (1980) and source information, compute ME_{FJ}

$$ME_{FJ} = \frac{kd_{PS}}{\bar{c}}\left(\frac{\rho_{amb}}{\rho_{PS}}\right)^{\frac{1}{2}}$$

where $\bar{c}$ is the methane concentration of interest in air and k is the axial decay constant (equal to 4.4, as suggested by Birch et al. (1984)). Note that, the reliability of Chen and Rodi (1980) model is discussed elsewhere (Colombini et al., 2020a, Colombini et al., 2021a, Colombini et al., 2021c)

3. Coupling the models of Chen and Rodi (1980) and Cushman-Roisin (2020), estimate $d_{FJ}(D)$

$$d_{FJ}(D) = 2 \cdot \sqrt{-\frac{D^2}{50} \cdot \ln\left(\frac{\bar{c}}{c_{ax}(D)}\right)}$$

$$c_{ax}(D) = \frac{kd_{PS}}{D}\left(\frac{\rho_{amb}}{\rho_{PS}}\right)^{\frac{1}{2}}$$

where, D is the distance between the methane HP source and the cylindrical obstacle centre, $c_{ax}(D)$ is the methane concentration in correspondence of the spherical obstacle centre position, evaluated along the free jet axis. Colombini et al. (2021ac) discussed the reliability of the Cushman-Roisin (2020) model

4. If $d_{FJ}(D)$ / D_O < 1.8, ME can be roughly considered equal to ME_{FJ} since the maximum underestimation is expected to be lower than about 10%. If $d_{FJ}(D)$ / D_O ≥ 1.8, the results are outside the parameters window investigated, and thus the procedure expires its validity (see Figure 3)

Despite the CFD based analysis covered several hypothetical accidental scenarios, it should be remarked that the proposed procedure is expected to work out results with the stated accuracy inside the parameters window investigated. The use of CFD simulations might be always considered to confirm the estimated values, as well as to compute the results for those scenarios characterized by parameter values outside the investigated window.

3.3 OBSTACLE ORIENTATION ANALYSIS

In order to verify if the procedure proposed in previous Section can be valid also for cylindrical obstacles oriented vertically, a specific analysis was carried out considering runs 9_x-15_x of Table 3. Keeping the same geometrical characteristics of both source and tank (i.e., same H_N, D_O and L_O) as well as same HP methane release (i.e., p, T, d), the cylindrical obstacle was oriented vertically and located at the various distances (D) considered. Figure 4 sketches both the scenario. It has to be noted that, the height of the cylindrical obstacle oriented vertically, H_O, corresponds to the length of the one oriented horizontally, L_O.

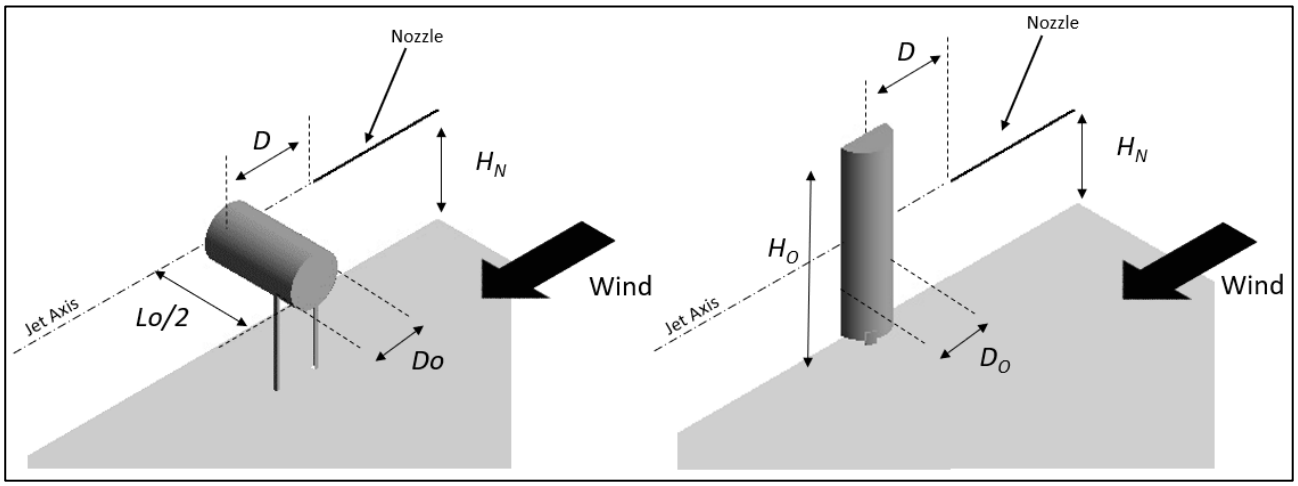

Figure 4: Representative sketches of the scenario involving horizontal and vertical cylindrical obstacle. In the Figure, the vertical symmetry plane in correspondence of the jet axis defines the boundary of the domain.

Figure 5, where the ratio ME/ME_{FJ} was plotted over the distances of the obstacle from the HP source, *D*, shows the obtained results.

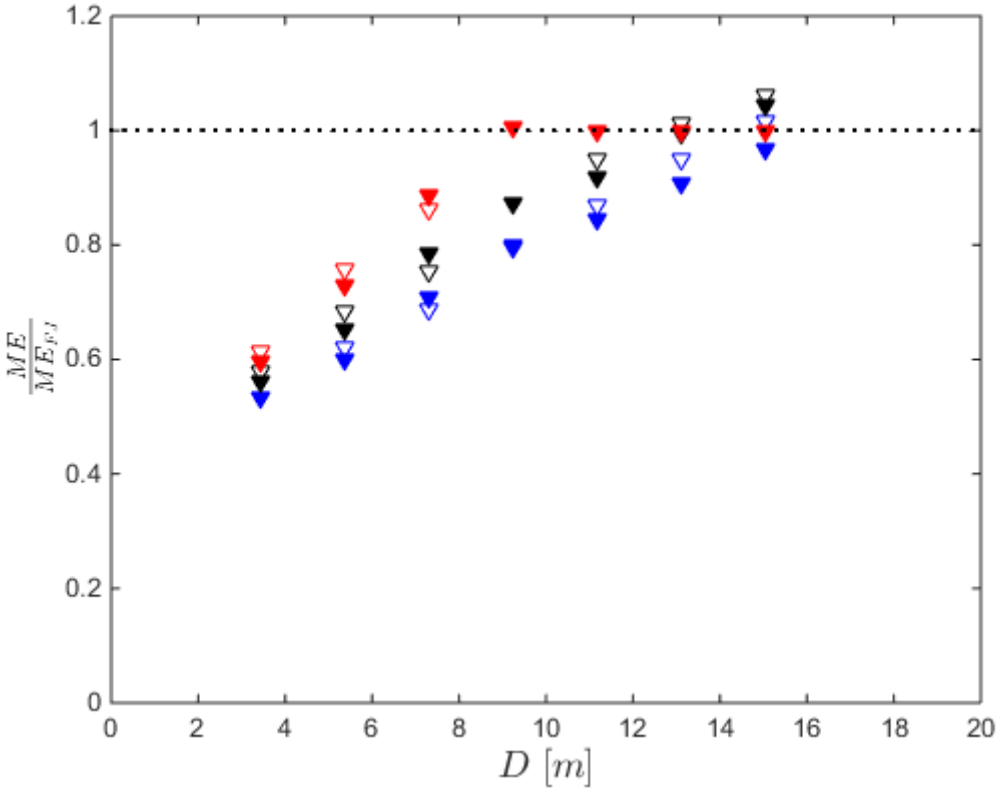

Figure 5: Comparison between vertical and horizontal orientation. Empty markers refer to vertical cylindrical obstacle while filled markers refer to horizontal cylindrical obstacle. Markers colour defines the methane concentration level observed: blue is for the low level (c = 3.5 %), black is for the mean level (c = 5.3 %) and red is for the high level (c = 10 %). The dotted line identifies when $ME/ME_{FJ} = 1$.

From Figure 5, we can see clearly that the obstacle orientation does not introduce any relevant effect in the jet development: the mean relative percentage difference with the results for the horizontal obstacle is equal to 2.2 %, with a maximum of 5 %).

4. CONCLUSIONS

The credible scenario of an unignited high-pressure methane jet impinging a cylindrical obstacle was extensively investigated. In total, 65 different scenarios were simulated by means of CFD computations. Observing 3 methane concentration levels, the cases analysed were 195. The analysis regarded horizontal cylindrical obstacles and vertical cylindrical obstacles. The main conclusions of the work are:

- With respect to what found for other kind of obstacles when impinged by a high-pressure jet (Colombini et al., 2020a, Colombini et al., 2020b; Colombini et al., 2021a; Colombini et al., 2021b; Colombini et al., 2021c), the cylindrical obstacle (be it oriented horizontally or vertically) has the effect of decreasing the jet maximum extent instead of increasing it; at most, the impinging jet results to have similar length of the free jet case;
- Within the parameters window considered, the simple procedure proposed in Section 3.2 can be used to quickly estimate, by order of magnitude, the hazardous area extent subsequent to the accidental release in the jet axis direction (which is, in principle, the worst case direction);

COMPETING INTERESTS STATEMENT

The Authors declare that there is no conflict of interest.

ACKNOWLEDGEMENTS

This research did not receive any specific grant from funding agencies in the public, commercial, or not-for-profit sectors.

REFERENCES

Angers, B., Hourri, A., Benard, P., Tchouvelev, A., 2011. Numerical investigation of a vertical surface on the flammable extent of hydrogen and methane vertical jets. *Int. J. Hydrogen Energy* 36, 2567-72.

Ansys DesignModeler User's Guide, 2017. Release 19.0. ANSYS, Inc.

Ansys Fluent User's Guide, 2017. Release 19.0. ANSYS, Inc.

Ansys Meshing User's Guide, 2017. Release 19.0. ANSYS, Inc.

Ansys Workbench User's Guide, 2017. Release 19.0. ANSYS, Inc.

Batt, R., Gant, S., Lacome, J., Truchot, B., 2016. Modelling of Stably-Stratified Atmospheric Boundary Layers with Commercial CFD Software for Use in Risk Assessment. *Chem. Eng. Trans.* 48, 61-66.

Bénard, P., Tchouvelev, A., Hourri, A., Chen, Z., Angers, B., 2007. High pressure hydrogen jets in the presence of a surface. *Int. Conf. Hydrog. Saf.* 40.

Bénard, P., Hourri, A., Angers, B., Tchouvelev, A., Agranat, V., 2009. Effects of surface on the flammable extent of hydrogen jets. *Int. Conf. Hydrog. Saf*.

Bénard, P., Hourri, A., Angers, B., Tchouvelev, A., 2016. Adjacent surface effect on the flammable cloud of hydrogen and methane jets: Numerical investigation and engineering correlations. *Int. J. Hydrogen Energy* 41, 18654–18662. https://doi.org/10.1016/j.ijhydene.2016.08.173.

Birch, A.D., Brown, D.R., Dodson, M.G., Swaffield, F., 1984. The structure and concentration decay of high pressure jets of natural gas. *Combust. Sci. Technol.* 36, 249–261. https://doi.org/10.1080/00102208408923739.

Casal, J., 2008. Evaluation of the Effects and Consequences of Major Accidents in Industrial Plants. Elsevier, Industrial Safety Series Vol. 8, Amsterdam, The Netherlands.

Casal, J., Gómez-Mares, M., Muñoz, M., Palacios, A., 2012. Jet fires: A 'minor' fire hazard? *Chem. Eng. Trans.* 26, 13–20. https://doi.org/10.3303/CET1226003.

Chen, C.J., Rodi, W., 1980. Vertical Turbulent Buoyant Jets – A review of Experimental Data, First ed. Pergamon Press Vol. 4.

Colombini, C., Busini, V., 2019a. Obstacle Influence on High-Pressure Jets based on Computational Fluid Dynamics Simulations. *Chem. Eng. Trans.* 77, 811–816. https://doi.org/10.3303/CET1977136.

Colombini, C., Busini, V., 2019b. High-Pressure Methane Jet: Analysis of the Jet-Obstcle Interaction. *Proceeding of the 29th European Safety and Reliability Conference.*

Colombini, C., Martani, A., Rota, R., Busini, V., 2020a. Ground influence on high-pressure methane jets: Practical tools for risk assessment. *J. Loss Prevent. Proc.* 67, 104240. https://doi.org/10.1016/j.jlp.2020.104240

Colombini, C., Carlini, L., Rota, R., Busini, V., 2020b. Ground Interaction on High-Pressure Jets: Effect on Different Substances. *Chem. Eng. Trans.* 82. https://doi.org/10.3303/CET2082062

Colombini, C., Maugeri G., Zanon, G., Rota, R., Busini, V., 2021a. Unignited High-Pressure Methane Jet Impinging a Pipe Rack: Practical Tools for Risk Assessment. *J. Loss Prevent. Proc. 69*, 104378. https://doi.org/10.1016/j.jlp.2020.104378

Colombini, C., Pontiggia, M., Uguccioni, G., Rota, R., Busini, V., 2021b. Ground Influence on High-Pressure Methane Jets: Different Concentration Clouds Scenarios. *Chem. Eng. Trans.* 86. Under Review.

Colombini, C., Carminati, E., Parisi, A., Rota, R., Busini, V., 2021c. Safety Evaluations on Unignited High-Pressure Methane Jets Impacting a Spherical Obstacle. *J. Loss Prevent. Proc.* Under Review.

Cushman-Roisin, B., Environmental Fluid Mechanics – John Wiley & Sons, Book in preparation. Last online access: August 2020. http://www.dartmouth.edu/~cushman/books/EFM/chap9.pdf

Darbra, R., Palacios, A., Casal, J., 2010. Domino effect in chemical accidents: Main features and accident sequences. *J. Hazard. Mater.* 183, 565–573

Deng, Y., Hu, H., Yu, B., Sun, D., Hou, L., Liang, Y., 2018. A method for simulating the release of natural gas from the rupture of high-pressure pipelines in any terrain. *J. Hazard. Mater.* 342, 418–428. https://doi.org/10.1016/j.jhazmat.2017.08.053.

Derudi, M., Bovolenta, D., Busini, V., Rota, R., 2014. Heavy gas dispersion in presence of large obstacles: Selection of modeling tools. *Ind. Eng. Chem. Res.* 53, 9303–9310. https://doi.org/10.1021/ie4034895.

Desilets, S., Cote, S., Nadau, G., Benard, P., Tchouvelev, A., 2009. Experimental results and comparison with simulated data of a low pressure hydrogen jet. *Int. Conf. Hydrog. Saf*.

Gerbec, M., Pontiggia, M., Antonioni, G., Tugnoli, a., Cozzani, V., Sbaouni, M., Lelong, R., 2017. Comparison of UDM and CFD simulations of a time varying release of LPG in geometrical complex environment. *J. Loss Prev. Process Ind.* 45, 56–68. https://doi.org/10.1016/j.jlp.2016.11.020.

Hall, J.E., Hooker, P., O'Sullivan, L., Angers, B., Hourri, A., Benard, P., 2017. Flammability profiles associated with high-pressure hydrogen jets released in close proximity to surfaces. *Int. J. Hydrogen Energy* 42, 7413–7421. https://doi.org/10.1016/j.ijhydene.2016.05.113.

Hess, K., Leukel, W., Stoeckel, A., 1973. Formation of explosive clouds on overhead release and preventive measure. *Chemie-Ingenieur-Technik* 45, 5.

Houf, W., Schefer, R., 2007. Predicting Radiative Heat Flux and Flammability Envelopes from Unintended Releases of Hydrogen. *Int. J. Hydrogen Energ.* 32, 136-151. https://doi.org/10.1016/j.ijhydene.2006.04.009

Houf, W., Schefer, R., Evans, G., Merilo, E., Groethe, M., 2010. Evaluation of barrier walls for mitigation of unintended releases of hydrogen. *Int. J. Hydrogen Energy* 35, 4758–4775. https://doi.org/10.1016/j.ijhydene.2010.02.086.

Hourri, A., Angers, B., Bénard, P., 2009. Surface effects on flammable extent of hydrogen and methane jets. *Int. J. Hydrogen Energy* 34, 1569–1577. https://doi.org/10.1016/j.ijhydene.2008.11.088.

Hourri, A., Angers, B., Bénard, P., Tchouvelev, A., Agranat, V., 2011. Numerical investigation of the flammable extent of semi-confined hydrogen and methane jets. *Int. J. Hydrogen Energy* 36, 2567–2572. https://doi.org/10.1016/j.ijhydene.2010.04.121.

Jang, C., Jung, S., 2016. Numerical computation of a large-scale jet fire of high-pressure hydrogen in process plant. *Energy Sci. Eng. 4(6), 406-417.*

Khraisheh, M., Almomani, F., Walker, G., 2020. Solid Sorbents as a Retrofit Technology for CO2 Removal from Natural Gas Under High Pressure and Temperature Conditions. *Sci. Rep.* 10, 269. https://doi.org/10.1038/s41598-019-57151-xx

Kotchourko, A., Baraldi, D., Bénard, P., Eisenreich, N., Jordan, T., Keller, J., Kessler, A., LaChance, J., Molkov, V., Steen, M., Tchouvelev, A., 2014. State of the Art and Research Priorities in Hydrogen Safety. Joint Research Centre of the European Commission (JRC), Honolulu, Hawaii.

Menter, F.R., 1993. Zonal Two Equation kω Turbulence Models for Aerodynamic Flows. *24th Fluid Dynamics Conference*.

Ozgoren, M., Pinar, E., Sahin, B., Akilli, H., 2011. Comparison of flow structures in the downstream region of a cylinder and sphere. *Int. J. Heat Fluid Fl.* 32, 1138-1146.

Pontiggia, M., Busini, V., Ronzoni, M., Uguccioni, G., Rota, R., 2014. Effect of large obstacles on high momentum jets dispersion. *Chem. Eng. Trans.* 36, 523–528. https://doi.org/10.1016/j.jhazmat.2009.06.064.

Pope, S. B., 2000. Turbulent Flows. Cambridge University Press, Cambridge. ISBN 978-0521598866.

Rian, K., Evanger, T., Vembe, B., Lilleheie, N., Lakså, B., Hjertager, B., Magnussen, B., 2016. Coherent computational analysis of large-scale explosions and fires in complex geometries – from combustion science to a safer oil and gas industry. *Chem. Eng. Trans* 48, 175-180 https://doi.org/10.3303/CET1648030

Sposato, C., Tamanini, F., Rogers, W.J., Sam Mannan, M., 2003. Effects of Plate Impingement on the Flammable Volume of Fuel Jet Releases. *Process Saf. Prog.* 22, 4. https://doi.org/10.1002/prs.680220406

Stewart, J.R., 2019. CFD modelling of underexpanded hydrogen jets exiting rectangular shaped openings. *Inst. Chem. Eng. Symp. Ser.* 2019-May.

Tchouvelev, A.V., Cheng, Z., Agranat, V.M., Zhubrin, S.V., 2007. Effectiveness of small barriers as means to reduce clearance distances. *Int. J. Hydrogen Energy* 32, 1409–1415. https://doi.org/10.1016/j.ijhydene.2006.10.020.

Tolias, I. C., Giannissi, S.G., Venetsanos, A.G., Keenan, J., Shentsov, V., Makarov, D., Coldrick, S., Kotchourko, A., Ren, K., Jedicke, O., Melideo, D., Baraldi, D., Slater, S., Duclos, A., Verbecke, F., Molkov, V., 2019. Best practice guidelines in numerical simulations and CFD benchmarking for hydrogen safety applications. *Int. J. Hydrogen Energy* 44, 9050–9062. https://doi.org/10.1016/j.ijhydene.2018.06.005.

Uggenti, A.C., Carpignano, A., Savoldi, L., Zanino, R., 2017. Perspective and criticalities of CFD modelling for the analysis of oil and gas offshore accident scenarios. *Risk, Reliability and Safety: Innovating Theory and Practice: Proceedings of ESREL 2016.*

Varsegova, E., Dresvyannikova, E., Osipova, L., Sadykov, R., 2019. Damage areas during emergency depressurization of a gas pipeline. *EECE Proceedings.* 140, 06007. https://doi.org/10.1051/e3sconf/201914006007

Woodward, J., Pitblado, R., 2010. LNG Risk Based Safety – Modeling and Consequences Analysis. John Wiley and Sons, Hoboken, New Jersey.

Xu, B.P., Wen, J.X., Tam, V.H.Y., 2011. The effect of an obstacle plate on the spontaneous ignition in pressurized hydrogen release: A numerical study. *Int. J. Hydrogen Energy* 36, 2637–2644. https://doi.org/10.1016/j.ijhydene.2010.03.143.

Zhang, Y., Zhu, J., Teng, L., Song, C., 2020. Experimental research of LNG accidental underwater release and combustion behavior. *J. Loss Prevent. Proc.* 64, 104036. https://doi.org/10.1016/j.jlp.2019.104036

Zhu, Y., Wang, D., Shao, Z., Zhu, X., Xu, C., Zhang, Y., 2020. Investigation on the overpressure of methane-air mixture gas explosions in straight large-scale tunnels. *Process Saf. Environ.* 135, 101-112. https://doi.org/10.1016/j.psep.2019.12.022